A high-performance aromatic polyimide fibre: 1. Structure, properties and mechanical-history dependence

Stephen Z. D. Cheng, Zongquan Wu, Mark Eashoo, Steven L. C. Hsu and Frank W. Harris

Institute and Department of Polymer Science, College of Polymer Science and Polymer Engineering, The University of Akron, Akron, OH 44325-3909, USA

(Received 11 August 1990; revised 2 November 1990; accepted 12 November 1990)

A new segmented rigid-rod polyimide has been synthesized from 3,3',4,4'-biphenyltetracarboxylic dianhydride (BPDA) and 2,2'-bis(trifluoromethyl)-4,4'-diaminobiphenyl (PFMB). This polyimide is soluble in hot *m*-cresol, allowing fibres to be spun from an isotropic solution using a dry-jet wet spinning method. The as-spun fibres have low tenacities and low moduli, but they can be drawn at high temperatures (>380°C) under tension to large draw ratios (up to 10 times), which produces a remarkable increase in strength and modulus. Drawn fibres display a tensile strength of about 25 g den^{-1} (3.2 GPa) and an initial modulus higher than 1000 g den^{-1} (130 GPa). BPDA–PFMB fibres show excellent thermal stability and retain relatively high strength and modulus at elevated temperatures. Annealed BPDA–PFMB fibres display distinct wide-angle X-ray patterns, from which a monoclinic unit cell has been determined. Furthermore, changes in crystallographic *c*-axis, apparent crystal sizes, degree of crystallinity, crystal orientation and thermomechanical properties have been observed with different draw ratios.

(Keywords: apparent crystal size; aromatic polyimide; BPDA–PFMB fibres; crystal unit cell; crystallinity; degree of crystal orientation; modulus; tenacity; tensile strength; thermomechanical property)

INTRODUCTION

High-performance polymeric fibres with high-strength, high-modulus and high-temperature properties have undergone significant growth and development in the last two decades. In the late 1960s, the lyotropic liquid-crystalline behaviour of rigid-rod-like aromatic polyamides was discovered at Du Pont, which led to the development of Kevlar fibres[1–5]. At approximately the same time, several fibres were developed from aromatic polyhydrazides and polyamide hydrazides by Monsanto[1,2,6,7]. A few years later, high-performance fibres were obtained from thermotropic aromatic polyesters and copolyesters by Du Pont, Eastman Kodak, Hoechst Celanese and other companies[8–12]. In the mid-1970s, high-strength aromatic polyazomethine fibres were also developed[13,14]. The forefront of this evolution includes two major developments that occurred in the 1980s. One of these advances was the fabrication of aromatic heterocyclic polymers in high-performance fibres, such as poly(*p*-phenylenebenzobisthiazole) (PBZT) and poly(p-phenylenebenzobisoxazole) (PBO)[15,16]. The second was the preparation of high-performance aromatic polyimide fibres, which was mainly carried out by Japanese[17–25] and Soviet researchers[26–28]. An excellent review of the development of high-performance fibres has recently been provided by Yang[29].

The basic technology for forming synthetic fibres includes spinning and heat treatment. As is generally known, there are three major methods of spinning: melt, dry and wet spinning processes. The melt spinning process is employed widely for polymers that can be extruded in a molten state (either isotropic or anisotropic liquid state). The dry spinning process is carried out with solutions of polymers in volatile solvents. In this case, the solvent is recovered from the extruded filaments by flash vaporization upon contact with hot gases. The wet spinning process, so-called because water or aqueous solutions are often used as coagulating agents, is employed mostly for solutions of polymers in non-volatile solvents. The extrudate is passed directly into a non-solvent bath where fibre coagulation and solvent extraction take place. Some combinations of two spinning methods are also used, such as the dry-jet wet spinning method used in the production of Kevlar, PBZT and PBO fibres. In this process, the polymer solution is passed through a short air gap prior to immersion in the coagulation bath.

Following spinning, a fibre is heat treated by one of three methods: (1) free end annealing, (2) fixed end annealing or (3) annealing under tension. Generally speaking, the heat treatment is applied to improve the fibre strength and/or modulus. From a molecular point of view, various spinning methods and heat treatment processes affect the chain orientation, crystallinity, crystal sizes and morphologies in the fibres. These are the basic structure parameters in fibres that are usually characterized by various analytical methods. On the other hand, macroscopic thermal, mechanical and chemical properties can also be measured. However, the establishment of relationships between structure, properties and processing conditions is still an unfinished task in high-performance fibres.

In this paper, we report our recent work with an

Paper presented at Speciality Polymers '90, 8–10 August 1990, The Johns Hopkins University, Baltimore, MD, USA

0032-3861/91/101803-08

advanced high-performance polyimide fibre. The polyimide was synthesized from 3,3′,4,4′-biphenyltetracarboxylic dianhydride (BPDA) and 2,2′-bis(trifluoromethyl)-4,4′-diaminobiphenyl (PFMB) in *m*-cresol[30]. Its chemical structure is:

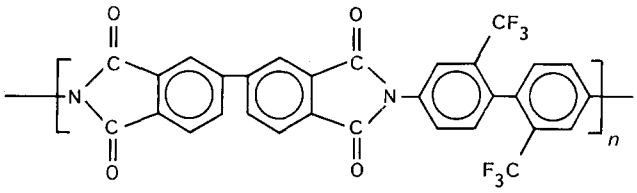

with a molecular mass of 578.5 g mol^{-1} per repeat unit. This undertaking deals with the characterization of the structures of the BPDA–PFMB fibres produced from isotropic solutions by dry-jet wet spinning and the evolution of their thermal and mechanical properties. Details of the spinning process, the fibre formation mechanism through gelation and heat treatment process will be discussed in later publication(s)[31].

EXPERIMENTAL

Materials

The polymer was prepared by the polymerization of an aromatic dianhydride (BPDA) with a diamine (PFMB) in *m*-cresol using different solid concentrations at high temperatures[30]. The polymer with the highest monomer concentration (15% (w/w)) remained completely in solution during the polymerization until it was cooled below about 100°C. Near this temperature the solution formed a gel, accompanied by the development of a lyotropic liquid-crystal state. A detailed description of mechanisms of gel–sol and liquid-crystal transitions has been published elsewhere[32]. The intrinsic viscosity of the BPDA–PFMB in *m*-cresol at 30°C was 4.9 dl g^{-1}.

Fibre spinning process

A schematic of the spinning apparatus is shown in *Figure 1*. Fibres from isotropic solutions of 12–15% polymer in *m*-cresol were dry-jet spun into a coagulation bath of water/methanol. The as-spun fibres were drawn at different temperatures and different draw ratios in air.

Equipment and experiments

Wide-angle X-ray diffraction (WAXD) experiments were conducted using a Rigaku X-ray generator with a 12 kW rotating anode. The point-focused beam was monochromatized by a graphite crystal sensitive to Cu K_α radiation. X-ray fibre diagrams were photographed by a vacuum camera in order to determine crystal structure. The *d* spacings were calibrated with silicon powder (325 mesh size). To observe the difference of *d* spacings for varying draw ratios, the fibre diagrams were also recorded along both meridional and equatorial directions by a Rigaku diffractometer.

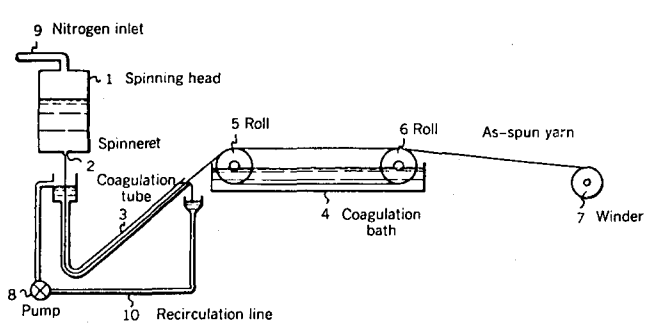

Figure 1 A schematic illustration of a dry-jet wet spinning apparatus

X-ray crystallinity determinations of the fibres were carried out by subtraction of the background, which corresponds to the WAXD pattern of the amorphous glass obtained from as-spun fibres without any drawing during spinning.

Crystal orientations in the fibres were measured based on the Hermans equation:

$$f_c \times 100\% = (3\langle\cos^2\phi_c\rangle - 1)/2 \quad (1)$$

where f_c is the orientation factor along the fibre direction and ϕ_c represents the angle between the fibre axis and the *c* axis of the crystal unit cell. Since the (003) crystallographic plane of the fibres along the meridional direction is the most isolated and clear diffraction spot, the numerical values for the mean-square cosine in equation (1) can be determined from the fully corrected intensity distribution diffracted from the (003) crystallographic planes and $I_c(\phi_c, \alpha)$, averaged over the entire surface of the orientation sphere:

$$\langle\cos^2\phi_c\rangle = \frac{\int_0^{\pi/2}\int_0^{2\pi} I_c(\phi_c, \alpha)\cos^2\phi_c \sin\phi_c \, d\alpha \, d\phi_c}{\int_0^{\pi/2}\int_0^{2\pi} I_c(\phi_c, \alpha)\sin\phi_c \, d\alpha \, d\phi_c} \quad (2)$$

Determination of the apparent crystal size in the fibres perpendicular to the (310) and (003) crystallographic planes was conducted by use of the Scherrer equation:

$$L = K\lambda/[(\beta^2 - b^2)^{1/2}] \quad (3)$$

where β and b are, respectively, the halfwidth of the (310) or (003) plane diffraction peak and the broadening factor ($b = 0.5$, which was determined by equipment calibration), and K is a geometry-dependent constant that is assumed to be unity.

The density measurements were conducted on a gradient density column using a hexane–carbon tetrachloride system at 25°C. This allowed for measurements of density in the range of 1.40–1.50 g cm^{-3}.

The mechanical property experiments were carried out on an Instron mechanical analyser at 25°C. Compliance corrections were performed. Stress–strain relationships were obtained for the as-spun fibres and the fibres that were drawn to different draw ratios.

Thermal gravimetry analysis (t.g.a.) was performed on a Du Pont TGA 951. Powdered polyimide samples were subjected to a heating rate of 10°C min^{-1} under both air and dry nitrogen atmospheres.

Thermomechanical properties of the fibres were determined on a Seiko stress–strain thermal mechanical analyser (TMA/SS 100). A single fibre was clamped into the sample holder with a small initial stress in order to keep the fibre straight. This initial stress was approximately 1 mg den^{-1} (1.28 MPa). Two different modes were used in this analysis: (1) measurement of the change in stress at constant fibre length and (2) the change in fibre length at constant stress. The frequency of each cycle was 1 Hz, with a heating rate of 10°C min^{-1}.

RESULTS AND DISCUSSION

Crystal unit-cell determination

Figures 2a and *2b* are typical crystal diffraction photographs of a highly drawn ($\lambda=8$) BPDA–PFMB fibre obtained at different exposure times. Along the equator, there are four diffraction spots that can be identified. Along the meridian, periodic diffraction spots can be clearly observed for up to six layers. On the quadrants, one spot along the first, the second and the third layers, and two along the fourth layer can be seen. A detailed listing of the 12 experimental 2θ angles, d spacings and the corresponding intensities of the diffraction spots is given in *Table 1*. The streaks in *Figures 2a* and *2b* may be caused by crystal disorder. It should be pointed out that the fluorine atoms in the pendant perfluoromethyl groups absorb the X-rays, and influence diffraction intensities.

To determine the size and shape of the crystal unit cell responsible for a diffraction pattern, one ordinarily begins by trying to find an $hk0$ reciprocal lattice net, namely a parallelogram with edges a^* by b^* that accounts for the values determined from the equatorial diffractions. The smallest distance between the centre of the X-ray incident beam and the diffraction spot corresponds to a low index. From *Figure 2*, the $hk0$ reciprocal lattice net can be formed if the diffraction spot of $2\theta=17.25°$ is assigned as (310) crystallographic planes. All the other diffraction spots can be fitted into this net. The l index of each diffraction can also be determined by the layer line on which the diffraction lies. The c crystallographic axis is readily determined from the layer-line spacing. After least-squares refinements with a computer, we found that the crystal unit cell of the highly drawn BPDA–PFMB fibre is monoclinic with $a=15.40$ (±0.04) Å, $b=9.90$ (±0.04) Å, $c=20.25$ (±0.05) Å and $\gamma=56°$ ($\pm0.2°$). This corresponds to a crystallographic volume of 2559.2 Å^3 containing four repeat units. The calculated crystallographic density is thus 1.501 g cm^{-3}. The experimental density was found to be in the range of 1.45–1.47 g cm^{-3} (see below). All the calculated and experimentally observed d spacings for each hkl crystal plane have also been listed in *Table 1* for comparison. A similar crystal structure has been reported for a polyimide fibre prepared from BPDA and 3,4′-diaminodiphenyl ether (DADE). In this case, the polymer has a monoclinic unit cell[33] with $a=14.8$ Å, $b=8.20$ Å, $c=20.6$ Å and $\gamma=56°$.

Crystal structures of other BPDA-based polyimides have also been reported. Oda studied the WAXD pattern of a polyimide fibre prepared from BPDA and *p*-phenylenediamine (BZDA). He found that the crystal unit cell was monoclinic[33] with a c axis of 16.0 Å. For BPDA-based polyimides, one may consider two different chain conformations based on the rotation of the C–C bond between the two BPDA phenyl rings. For the BPDA–BZDA fibres, the planar *cis* conformation leads to a chain repeat distance of 15.2 Å and the *trans* conformation to a distance of 16.2 Å. *Figure 3* shows the planar conformations of one repeat unit in a single BPDA–PFMB chain. Because of the steric interferences between the hydrogen atoms located *ortho* to the connecting linkage on the opposing phenylene rings of BPDA, these planar conformations are difficult to form. Thus, the phenylene rings must twist away from the

Table 1 Experimental and calculated crystallographic parameters of the monoclinic crystal unit cell for BPDA–PFMB fibres[a]

	2θ (deg)		d spacing (Å)		
(hkl)	Exp.	Calc.	Exp.	Calc.	Intensity[b]
100	6.881	6.923	12.84	12.76	w
200	13.90	13.87	6.371	6.384	w
310	17.25	17.29	5.140	5.127	s
420	23.82	23.90	3.735	3.723	m
101	8.167	8.186	10.82	10.80	w
102	11.24	11.15	7.872	7.933	m
003	13.08	13.11	6.768	6.750	vs
013	16.99	17.01	5.218	5.213	m
004	17.63	17.52	5.030	5.063	s
104	18.70	18.85	4.744	4.706	s
014	20.70	20.61	4.291	4.309	m
006	26.42	26.41	3.073	3.375	m

[a] The calculated data for 2θ and d spacing are based on a monoclinic crystal unit cell of $a=15.40$ Å, $b=9.90$ Å, $c=20.25$ Å and $\gamma=56°$

[b] Intensity was semiquantitatively measured through a microdensitometer, and classified by very strong (vs), strong (s), medium (m) and weak (w)

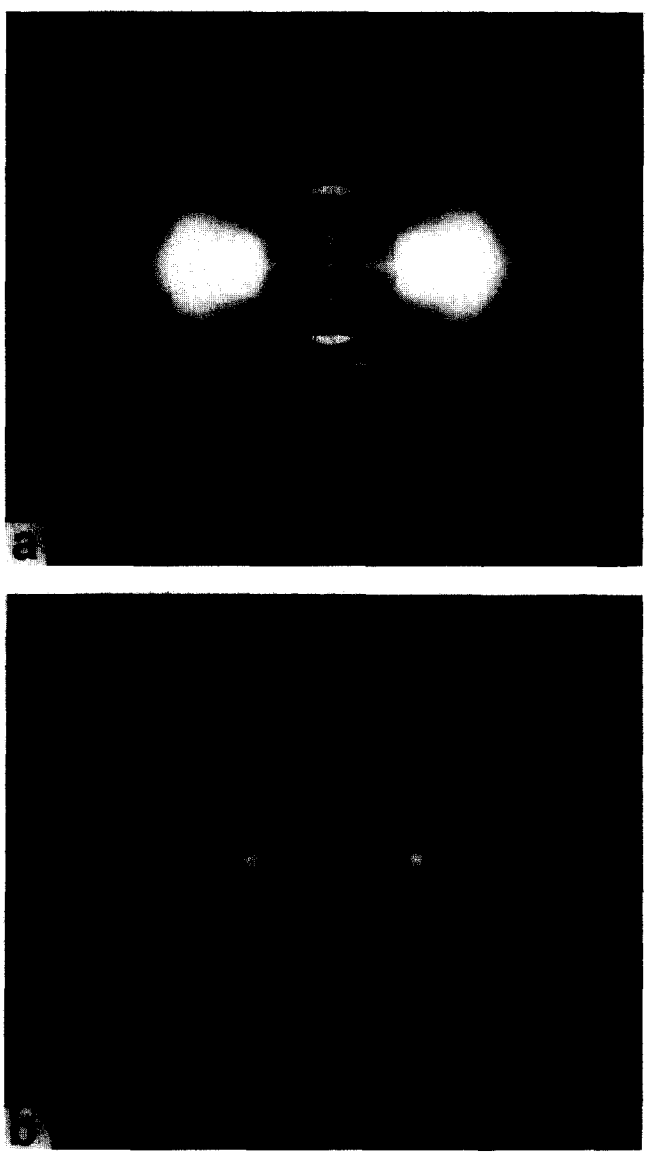

Figure 2 Typical photographs of WAXD patterns of highly drawn ($\lambda=8$) BPDA–PFMB fibres: (a) 48 h exposure time; (b) 12 h exposure time

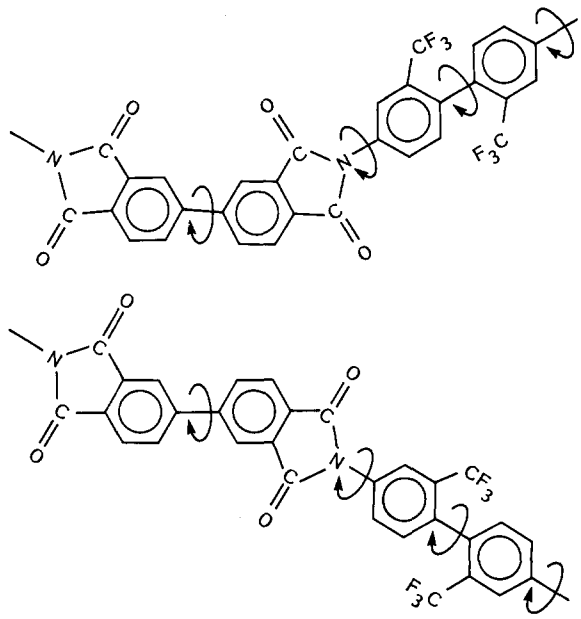

Figure 3 Two different conformations of one repeat unit in BPDA–PFMB single chain molecule (planar *trans* and *cis*)

planar position to minimize the rotational conformational energy. According to Oda's analysis, the 16.0 Å *c* axis was a result of a 60° twist of the phenylene rings in the BPDA *trans* conformation[33]. A similar twist between the two aromatic rings in BPDA has also been found in preliminary computer modelling studies of a single chain set at the lowest rotational conformational energy[34] and other polyimides[35].

Furthermore, it has also been reported that for the fibres of aromatic polyimides synthesized from pyromellitic dianhydride (PMDA) and different diamines containing one phenylene ring (BZDA), two phenylene rings (4,4′-diaminobiphenyl) and three phenylene rings (4,4″-diaminoterphenyl), the crystal unit cells only change along the *c* axes. Each additional phenylene ring leads to an increase of about 4.3–4.4 Å in the *c* axes[36]. Based on these results and the data obtained for BPDA–BZDA, the *c* axis of the unit cell in the BPDA–PFMB fibres should be 20.3–20.4 Å (16.0 Å + 4.3 or 4.4 Å). As stated earlier, the *c* axis is observed to be 20.25 Å in the unit cell. The experimental value is slightly smaller than the predicted length, and is perhaps due to further twisting of the chain caused by the presence of the two trifluoromethyl groups in PFMB[34].

Of special interest is that the *c* axis of the crystal unit cell can be linearly correlated with the mechanical history, i.e. the macroscopic draw ratio. *Figure 4* shows the WAXD patterns along the meridian for fibres with different draw ratios. It is evident that, as the draw ratio increases, the diffraction peak of the (003) crystallographic plane shifts to a lower angle. At the same time, the halfwidth of the peak, β, decreases. The shift of the diffraction peak indicates that the length of the *c* axis increases as the draw ratio increases, as shown in *Figure 5*. This also indicates that the lattice strain, which was frozen in the crystal unit cell after the fibres were drawn at high temperatures, is proportional to the draw ratio. Such strain can be released by a subsequent annealing process. A similar observation has been reported recently on Kevlar fibres[37].

Apparent crystal sizes

By applying the Scherrer equation (equation (3)), the fibres' apparent crystal sizes can be calculated. *Figure 6* illustrates the changes in apparent crystal sizes along two different crystallographic planes, i.e. (310) and (003), that take place as the fibre is drawn. It should be noted that these two apparent crystal sizes are representative of different directions in the fibres. The apparent crystal size along the (003) plane is along the fibre (or chain)

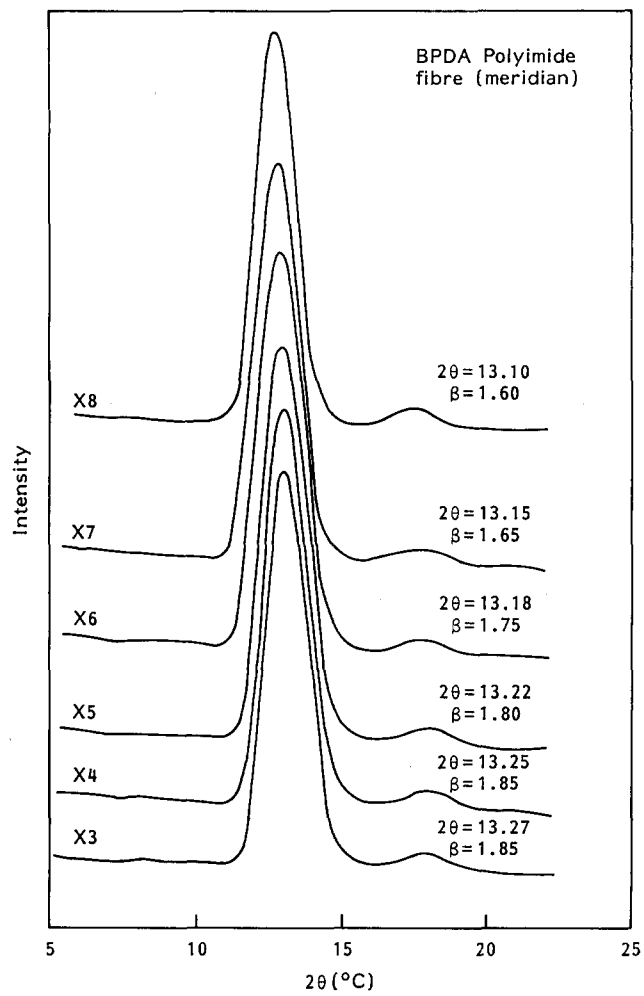

Figure 4 A set of WAXD patterns along the meridian at different draw ratios. The values of β represent the halfwidths of the (003) diffraction peaks

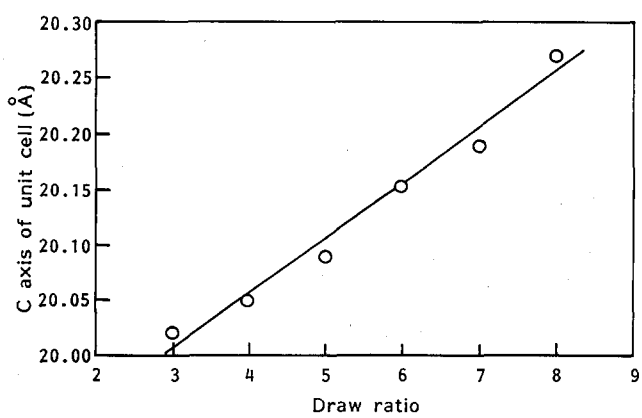

Figure 5 A linear relationship between the length of *c* axis in crystal lattice and different draw ratios

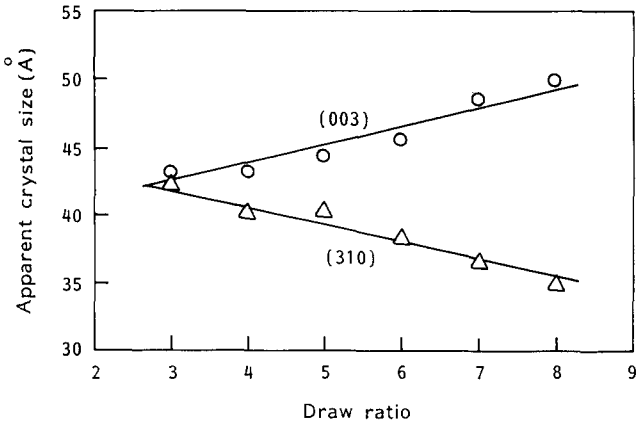

Figure 6 Apparent crystal sizes along (310) and (003) crystallographic planes change linearly with different draw ratios

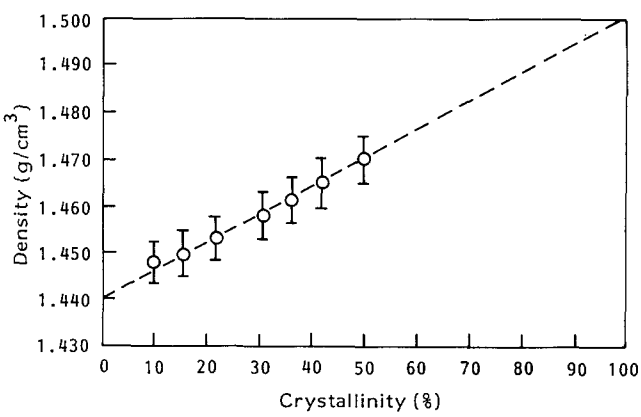

Figure 7 A relationship of the density with respect to the degree of crystallinity in the BPDA–PFMB fibres

direction, while that along the (310) plane is perpendicular to the fibre direction. It is surprising that, as the draw ratio increases, the apparent crystal size along the (003) plane increases, but that along the (310) plane decreases. The relationships shown in *Figure 6* may also indicate changes in the crystal morphology in the fibre during the drawing. At a high draw ratio, the fibre apparently develops a relatively perfect crystal structure along the chain direction, but perpendicular to the chain direction the crystal structure breaks down. Small crystals separated by amorphous defects may serve as a reasonable description.

Crystallinity and density measurements

Figure 7 illustrates the relationship between the degree of crystallinity and the density in the BPDA–PFMB fibres. Owing to different draw ratios, the fibres show a wide range of crystallinities. As-spun fibres have very low degrees of crystallinity (about 10%), while highly drawn fibres exhibit a crystallinity of about 50% based on WAXD data. As stated earlier, the crystallographic density for perfect crystallinity (100%) was calculated to be 1.501 g cm^{-3}. The density of a totally amorphous material was estimated by extrapolating the data in *Figure 7* to 0% crystallinity. As shown in the figure, this value is 1.440 g cm^{-3}. The difference between these two densities is surprisingly small compared with other semicrystalline polymers, which usually show a difference of about 0.1 g cm^{-3} between these two states[38]. This leads to a speculation that the lateral molecular packing in these two states may not be as different as in other flexible semicrystalline polymers in the range of one repeat unit length. This could be due to the rigid nature of the chain, as observed in poly(4,4′-oxydiphenylene-pyromellitimide)[39].

Crystal orientation

Using equations (1) and (2), one can determine the crystal orientation in the fibre. *Figure 8* shows the relationship between the crystal orientation factor obtained from WAXD experiments and the draw ratio. It is evident that the crystal orientation increases with draw ratio. In particular, at a draw ratio of $\lambda = 3$, a crystal orientation factor of 75% was achieved. This indicates that the polymer molecules are relatively easy to align, which is a result of the chain rigidity. Therefore, the crystal orientation is high. Above $\lambda = 7$, the orientation factor reaches about 87%. Further increases in the draw ratio lead to a minor increase in this factor. This value is comparable with the crystal orientation factors of other fibres such as Kevlar[37], which have values of 80–90%.

Tensile stress–strain experiments

Figure 9 shows the relationship between the tensile stress and the fibres' strain to break at room temperature. For as-spun fibres, the stress to break is around 2.7 g den^{-1} (0.35 GPa) with a large elongation (strain) of up to 60%. With increasing draw ratios, the stress increases remarkably. Thus, it reaches 10.2 g den^{-1} (1.3 GPa) at $\lambda = 3$ and 25 g den^{-1} (3.2 GPa) at $\lambda = 8$. After a draw ratio of $\lambda = 7$, the stress to break remains almost constant. Correspondingly, the tensile strain to break decreases from 8–10% at $\lambda = 3$ to 3–4% at $\lambda = 8$.

The initial modulus calculated from the ratio of the tensile stress and strain shows a drastic increase as the draw ratio increases. As-spun fibres have an initial modulus of 4.50 g den^{-1} (0.58 GPa), which increases to 126 g den^{-1} (16.3 GPa) at $\lambda = 3$ and then reaches 830 g den^{-1} (107 GPa) at $\lambda = 8$. Further increasing the draw ratio does not increase the tensile stress to break, but the tensile strain is continuously decreased, which results in the initial modulus being increased to 1000 g den^{-1} (130 GPa). This behaviour is different from that displayed by fibres spun from liquid-crystalline states, such as Kevlar fibres[37] and PBZT fibres[15,16]. In these cases, as-spun fibres have relatively high strength and modulus. Since the BPDA–PFMB fibre is spun from

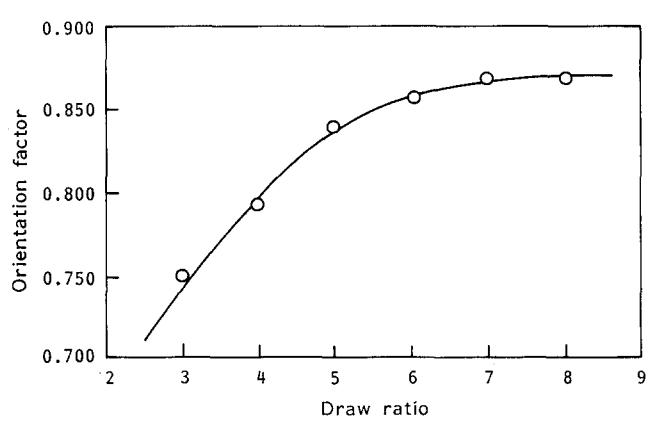

Figure 8 A relationship between crystal orientation factor and draw ratio

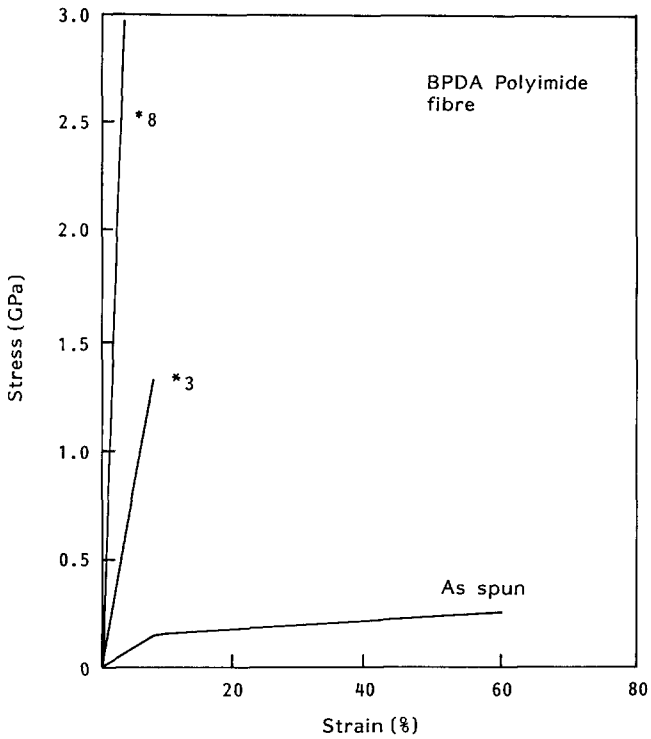

Figure 9 Typical stress–strain diagrams to break for the BPDA–PFMB fibres at different draw ratios (as spun, $\lambda = 3$ and $\lambda = 8$)

an isotropic solution rather than from a lyotropic liquid-crystalline state, the chain molecules are not fully oriented and crystallized in the as-spun fibres. As a result, the fibres can undergo considerable elongation during drawing (*Figure 9*) compared to Kevlar and PBZT fibres. The advantage of this spinning method is that, during the drawing process, the chain molecules have a better opportunity to rearrange themselves into defect-free positions under the large deformation. Ozawa observed that an aromatic polyamide fibre spun from an isotropic solution and then drawn at elevated temperature to $\lambda = 10$ showed much higher base and acid resistance compared to Kevlar and aromatic polyester fibres[40]. He attributed this behaviour to higher crystalline perfection in the drawn fibres.

Thermal stability of the fibres

Thermal gravimetric analysis (t.g.a.) thermograms of powdered BPDA–PFMB samples show a 5% weight loss under dry nitrogen and air atmospheres at 600°C (*Figure 10*). Thus, the polymer has excellent thermal stability. However, for polymeric fibres one is more interested in the retention of their mechanical properties, such as initial tensile strength, modulus, etc., at elevated temperatures. *Figure 11* shows how the highly drawn BPDA–PFMB fibres retain their modulus at 400 and 420°C. These experiments were conducted using an elongation fatigue mode at 1 Hz under a stress of 1 g den^{-1} (0.13 GPa). It is evident that at these temperatures the loss of modulus is not serious before the fibres break. For example, at $T_a = 420$°C, the initial modulus loss is about 15% over 1.5 h, while at $T_a = 400$°C, almost 93% of the modulus is retained for 3 h. This performance is far superior to that of Kevlar fibres under the same conditions. (At $T_a = 420$°C, the modulus of Kevlar fibres drops to zero within 15 min.)

Figure 12 illustrates the retention of modulus of the BPDA–PFMB fibres with different draw ratios ($\lambda = 5$ and 8) when heated at a constant rate of 10°C min^{-1}. As the draw ratio increased, the fibre's modulus retention increases at constant temperature. This indicates that the drawing process after the fibres have been spun is very

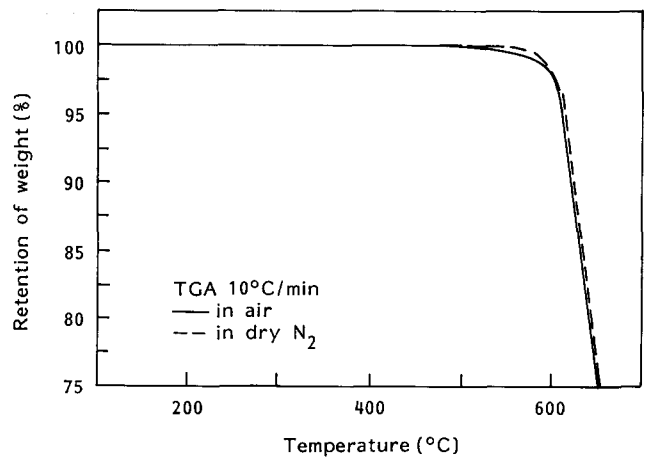

Figure 10 T.g.a. diagrams of the bulk BPDA–PFMB polyimides under air and dry nitrogen atmosphere heated at 10°C min^{-1}

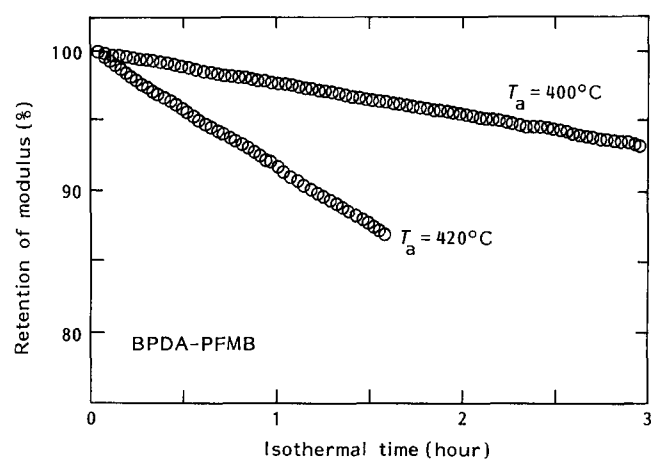

Figure 11 Changes of retention of modulus in the BPDA–PFMB fibres at isothermal temperatures of 400 and 420°C with time under elongation fatigue tests

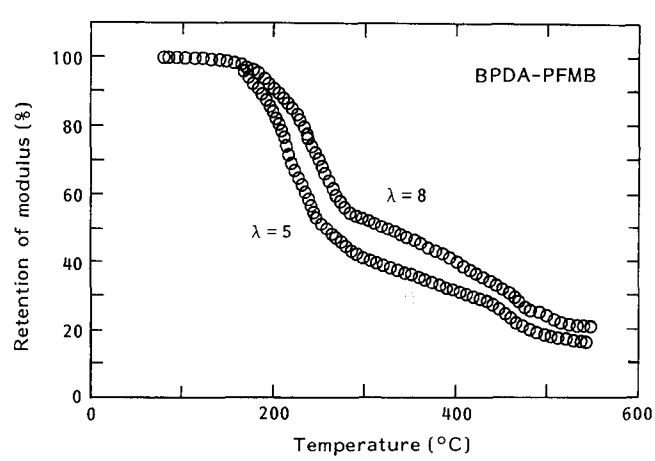

Figure 12 Changes of retention of modulus during heating at a constant rate of 10°C min^{-1} under elongation fatigue tests

important. High draw ratios are necessary to maintain good mechanical properties at elevated temperatures. Special attention should be paid to the temperature region where relatively large decreases of modulus become evident. For the BPDA–PFMB fibre, as shown in *Figure 12*, this decrease starts at around 200°C. This observation may suggest that 200°C is the starting temperature where segmental motion in the chain molecules begins. At about 250°C, half of the initial modulus value at room temperature is kept. Again, these temperatures increase with increasing draw ratio. Furthermore, the decrease of the modulus caused by the segmental motion is also draw-ratio-dependent. This is a clear indication that crystallinity influences the mechanical properties, since the crystallinity in the fibre is closely related to the draw ratio, as shown in *Figure 7*.

It should also be pointed out that, while the fibres studied were put through heated deformation processes, they were not subsequently heat treated. Further annealing at elevated temperatures may lead to an improvement of the thermomechanical properties, in particular, in the temperature region between 200 and 500°C.

Thermal shrinkage properties

Figures 13 and *14* show the thermal shrinkage stress and strain developed in BPDA–PFMB fibres with different draw ratios as they are heated at a constant rate of 10°C min^{-1}. From *Figure 13*, it is evident that the thermal shrinkage stress starts increasing at about 240°C for the fibre with a draw ratio of $\lambda = 3$. This temperature shifts to 300°C for the fibre with $\lambda = 7$. Furthermore, the amount of thermal shrinkage stress decreases with increasing draw ratio, revealing a crystallinity dependence of this stress. It is interesting that the appearance of the thermal shrinkage strain shown in *Figure 14* corresponds well to that of the shrinkage stress in *Figure 13*, although these two experiments were performed independently. One can clearly observe that the thermal shrinkage strain increases at about the same temperature as the thermal shrinkage stress for each fibre sample (*Figure 14*). This indicates that the thermal shrinkage behaviour is caused by segmental motion as described previously. Needless to say, this strain is negative since the fibre has a negative thermal expansion coefficient.

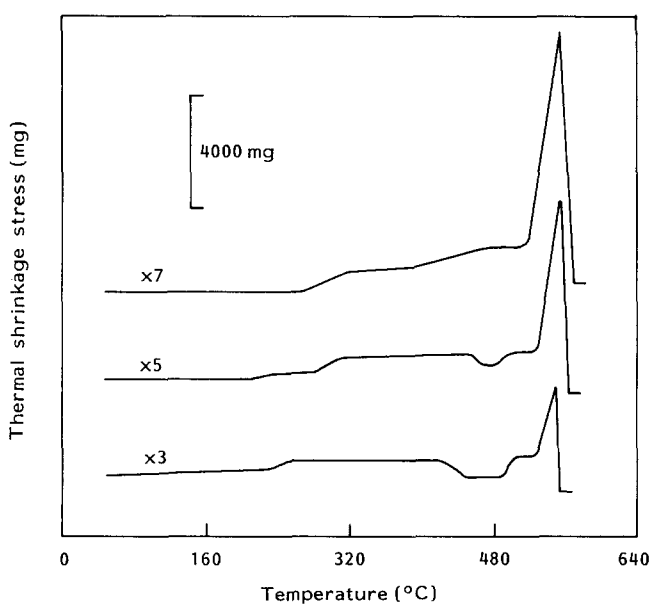

Figure 13 Thermal shrinkage stress measurements of the BPDA–PFMB fibres at different draw ratios under a constant fibre length

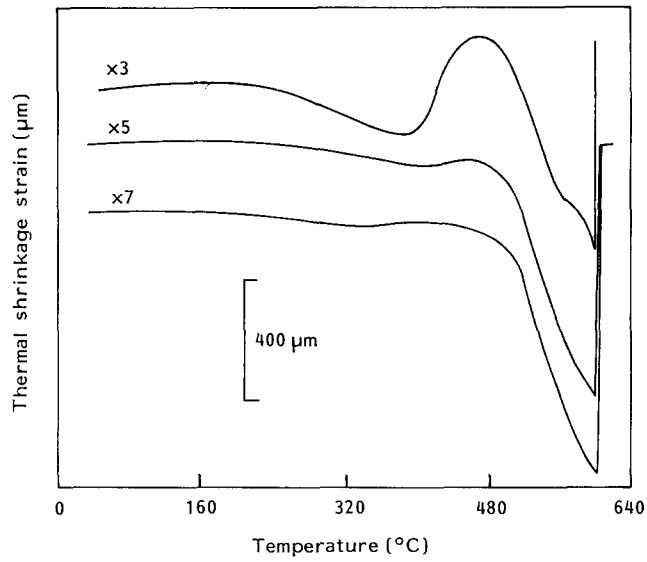

Figure 14 Thermal shrinkage strain measurements of the fibres at different draw ratios under a constant initial stress (the stress is small in order to keep the fibre straight)

Another process takes place near 460°C in the fibres with low draw ratios ($\lambda = 3$ and 5); at this point, the thermal shrinkage stress is reduced and, correspondingly, the thermal shrinkage strain is decreased, indicating an extension process. Microscopically, this corresponds to a crystallization process under tension, which was made clear by differential scanning calorimetry (d.s.c.) measurements on the fibres ($\lambda = 3$) at fixed length. An exothermic process can be clearly seen on the d.s.c. thermogram[31].

Finally, at even higher temperatures (around 600°C), the fibres break under tension. Both *Figures 13* and *14* show this process. We speculate that this process is associated with crystal melting under tension. This hypothesis was supported by d.s.c. experiments[31].

CONCLUSIONS

We have prepared a new high-performance aromatic polyimide fibre with high strength and high modulus. The fibre was dry-jet wet spun from an isotropic solution, and thus its mechanical properties were critically dependent upon a subsequent drawing process. The fibres with high draw ratios exhibited excellent thermal stability and retained good mechanical properties at elevated temperatures. The drawing process introduces thermal and mechanical histories to the fibre, and changes basic structure parameters of the fibre, such as crystal lattice dimensions, degree of crystallinity, density and crystal orientation. It is evident that the internal stress frozen in to the fibre during the drawing plays an important role in these parameter changes. Quantitatively studying the internal stress may lead to a further understanding of the relationship between structure and properties.

ACKNOWLEDGEMENTS

This work was supported by Edison Polymer Innovation Center (EPIC) through the study of polyimide composites. The synthesis of BPDA–PFMB (F.W.H. and S.L.C.H.) was also supported by a NASA Langley Research Center Grant (NAG-1-448).

REFERENCES

1 Black, W. B. and Preston, J. *J. Macromol. Sci.* (*A*) 1973, **7**, 3
2 Preston, J. *Polym. Eng. Sci.* 1975, **15**, 99
3 Kwolek, S. L. US Pat. 1972, 3 671 542; 1974, 3 819 587
4 Bair, T. I. and Morgan, P. W. US Pat. 1972, 3 673 143; 1974, 3 817 941
5 Blades, H. US Pat. 1973, 3 767 756; 1975, 3 869 429
6 Preston, J. US Pat. 1972, 3 632 548
7 Culkertson, B. M. and Murphy, R. *J. Polym. Sci.* (*B*) 1966, **4**, 249; 1967, **5**, 807
8 Jackson, W. J. and Kuhfuss, H. F. *J. Polym. Sci., Polym. Chem. Edn.* 1976, **14**, 2043
9 Acierno, D., LaMantia, F. P., Polizzotti, G., Ciferri, A. and Valenti, B. *Macromolecules* 1982, **15**, 1455
10 Calundann, G. W. US Pat. 1980, 4 184 996
11 Ueno, K., Sigimoto, H. and Hayatsu, K. US Pat. 1985, 4 503 005; EP Pat. 1985, 92 843
12 Krigbaum, W. R., Liu, C. K. and Yang, D. K. *J. Polym. Sci., Polym. Phys. Edn.* 1988, **26**, 1711
13 Morgan, P. W., Kwolek, S. L. and Pletcher, T. C. *Macromolecules* 1987, **20**, 729
14 Wojtkowski, P. W. *Macromolecules* 1987, **20**, 740
15 Allen, S. R., Filippov. A. G., Farris, R. J. and Thomas, E. L. *J. Appl. Polym. Sci.* 1987, **26**, 291
16 Allen, S. R., Filippov, A. G., Farris, R. J., Thomas, E. L., Wang, C. P., Berry, G. C. and Chenevey, E. C. *Macromolecules* 1981, **14**, 1135
17 Hara, S., Yamada, T. and Yoshida, T. US Pat. 1974, 3 829 399
18 Minami, M. and Taniguchi, M. US Pat. 1975, 3 860 559
19 Yokoyama, T., Miradera, Y., Shito, N., Suzuki, H. and Wakashima, Y. US Pat. 1977, 4 064 389
20 Sasaki, T., Itatani, H., Kashima, M., Yoshimoto, H., Yamamoto, S. and Sasaki, Y. US Pat. 1981, 4 247 443
21 Makino, H., Kusuki, Y., Harada, T. and Shimazaki, H. US Pat. 1983, 4 370 290; 1984, 4 460 526
22 Ohmura, K., Shihasaki, I. and Kimura, T. US Pat. 1983, 4 377 652
23 Ohta, T., Tanaga, Y. and Hino, S. US Pat. 1984, 4 438 256; EP Pat. 1983, 93 342
24 Nagaoka, K. US Pat. 1984, 4 448 957
25 Itatani, H., Inaike T. and Yamamoto, S. US Pat. 1986, 4 458 715
26 Koton, M. M. Br. Pat. 1970, 1 183 306; 1980, 2 025 311
27 Adrova, N. A., Bessenov, M. I., Louis, L. A. and Rudakoo, A. P. 'Polyimides', Technomic, Stamford, CT, 1970
28 Mittal, K. L. (Ed.) 'Polyimides', Plenum Press, New York, 1984
29 Yang, H. H. 'Aromatic High-Strength Fibers', Wiley, New York, 1989
30 Harris, F. W., Hsu, S. L. C. and Tso, C. C. *Polym. Prepr., Polym. Chem. Div. Am. Chem. Soc.* 1990, **31**(1), 342
31 Cheng, S. Z. D., Wu, Z.-Q., Eashoo, M., Hsu, S. L. C. and Harris, F. W. in preparation
32 Cheng, S. Z. D., Lee, S. K., Barley, J. S., Hsu, S. L. C. and Harris, F. W. *Macromolecules* in press
33 Kaneda, T., Katsura, T., Nakagawa, K., Makino, H. and Horio, M. *J. Appl. Polym. Sci.* 1986, **32**, 3151
34 Preliminary computer modelling results from Professor Mattice's laboratory
35 Whang, W. T. and Wu, S. C. *J. Polym. Sci., Polym. Chem. Edn.* 1988, **20**, 2749
36 Sidorovich, A. V., Baklagina, Yu. G., Kenarov, A. V., Nadezhin, Yu. S., Adrova, N. A. and Florinsky, F. S. *J. Polym. Sci., Polym. Symp.* 1977, **58**, 359
37 Wu. Z.-Q., Zhang, A.-Q., Cheng, S. Z. D., Wang, P. and Qian, B.-J. *J. Polym. Sci., Polym. Phys. Edn.* 1990, **28**, 2565
38 Wunderlich, B. 'Macromolecular Physics: Crystal Structure, Morphology, Defects', Academic Press, New York, Vol. 1, 1973
39 Takahashi, N., Yoon, D. Y. and Parrish, W. *Macromolecules* 1984, **17**, 2583
40 Ozawa, S. *Polym. J.* 1987, **19**, 119